1-6-2005

Analytical and Numerical Modeling of Soft Soil Stabilized by Prefabricated Vertical Drains Incorporating Vacuum reloading

Buddhima Indraratna
University of Wollongong, indra@uow.edu.au

I. Sathananthan
University of Wollongong

Cholachat Rujikiatkamjorn
University of Wollongong, cholacha@uow.edu.au

A. S. Balasubramaniam
Griffith University

Analytical and Numerical Modeling of Soft Soil Stabilized by Prefabricated Vertical Drains Incorporating Vacuum Preloading

B. Indraratna[1]; I. Sathananthan[2]; C. Rujikiatkamjorn[3]; and A. S. Balasubramaniam[4]

Abstract: This paper describes the analytical formulation of a modified consolidation theory incorporating vacuum pressure, and numerical modeling of soft clay stabilized by prefabricated vertical drains, with a linearly distributed (trapezoidal) vacuum pressure for both axisymmetric and plane strain conditions. The effects of the magnitude and distribution of vacuum pressure on soft clay consolidation are examined through average time-dependent excess pore pressure and consolidation settlement analyses. The plane strain analysis was executed by transforming the actual vertical drains into a system of equivalent parallel drain walls by adjusting the coefficient of permeability of the soil and the applied vacuum pressure. The converted parameters are incorporated in the finite element code *ABAQUS*, employing the modified Cam-clay theory. Numerical analysis is conducted to study the performance of a full-scale test embankment constructed on soft Bangkok clay. The performance of this selected embankment is predicted on the basis of four different vacuum pressure distributions. The predictions are compared with the available field data. The assumption of distributing the vacuum pressure as a constant over the soil surface and varying it linearly along the drains seems justified in relation to the field data.

DOI: 10.1061/(ASCE)1532-3641(2005)5:2(114)

CE Database subject headings: Soil consolidation; Finite element method; Plane strain; Soil improvement; Vertical drains; Preloading; Numerical models.

Introduction

Demand for infrastructure development on soft compressible soils continuously increases with the rise in population, especially in the coastal regions of many countries. Often, rapid development necessitates the utilization of even the poorest of soft clays; and therefore, it is essential to stabilize the existing soft clay foundations prior to construction, in order to avoid excessive and differential settlement. Even though there are a variety of soil improvement techniques available, the application of preloading with prefabricated vertical drains (PVD) is still regarded as one of the classical and popular methods in practice.

Preloading is the application of surcharge load on the site prior to the construction of the permanent structure, until most of the primary consolidation has occurred. Since compressible soils are usually characterized by very low permeability, the time needed for the desired consolidation can be long, even with a relatively high surcharge load. Therefore, the application of preloading alone may not be feasible with tight construction schedules, hence, a system of geosynthetic PVD is often introduced to achieve accelerated radial drainage and consolidation.

The behavior of soft clay foundations stabilized with vertical drains can now be predicted with acceptable accuracy due to significant progress that has been made in the past decade through rigorous numerical analysis. The first conventional procedure for radial consolidation by vertical drains was proposed by Baron (1948), which was later modified by various researchers including Kjellman (1952), Yoshikuni and Nakanodo (1974), Onoue (1988), and Zeng and Xie (1989). The effectiveness of PVD in accelerating consolidation for improved embankment stability has been well described by Jamiolkowski and Lancellotta (1984), and Holtz and Christopher (1987). A rigorous "unit cell" approach incorporating both the smear effect and well resistance has been conducted by Hansbo (1981). Similar studies have often been executed in the prediction of settlement along the embankment centerline, where the highest settlement is expected. Subsequently, Hird et al. (1992) introduced a unit cell formulated for the two-dimensional (2D) plane strain condition, which can be conveniently simulated in numerical modeling. Due to the common usage of plane strain finite element analysis, Indraratna and Redana (1997) extended the equivalent unit cell theory to convert the axisymmetric parameters such as permeability coefficient into equivalent plane strain parameters.

Application of vacuum pressure with surcharge load along the surface, in the absence of vertical drains, was modeled by Mohamedelhassan and Shang (2002), based on one-dimensional (1D) consolidation. The usefulness of the vacuum pressure application in practice was discussed by Qian et al. (1992), Cognon et al. (1994), Chu et al. (2000), and Eriksson et al. (2000). The appli-

[1]Professor, Division of Civil Engineering, Faculty of Engineering, Univ. of Wollongong, Wollongong City, NSW 2522, Australia (corresponding author). E-mail: indra@uow.edu.au

[2]PhD Candidate, Division of Civil Engineering, Univ. of Wollongong, Wollongong City, NSW 2522, Australia.

[3]PhD Candidate, Division of Civil Engineering, Univ. of Wollongong, Wollongong City, NSW 2522, Australia.

[4]Professor, School of Engineering, Griffith Univ., Gold Coast, QLD 4111, Australia; formerly, Asian Institute of Technology, Bangkok, Thailand.

Note. Discussion open until November 1, 2005. Separate discussions must be submitted for individual papers. To extend the closing date by one month, a written request must be filed with the ASCE Managing Editor. The manuscript for this paper was submitted for review and possible publication on February 9, 2004; approved on July 22, 2004. This paper is part of the ***International Journal of Geomechanics***, Vol. 5, No. 2, June 1, 2005. ©ASCE, ISSN 1532-3641/2005/2-114–124/$25.00.

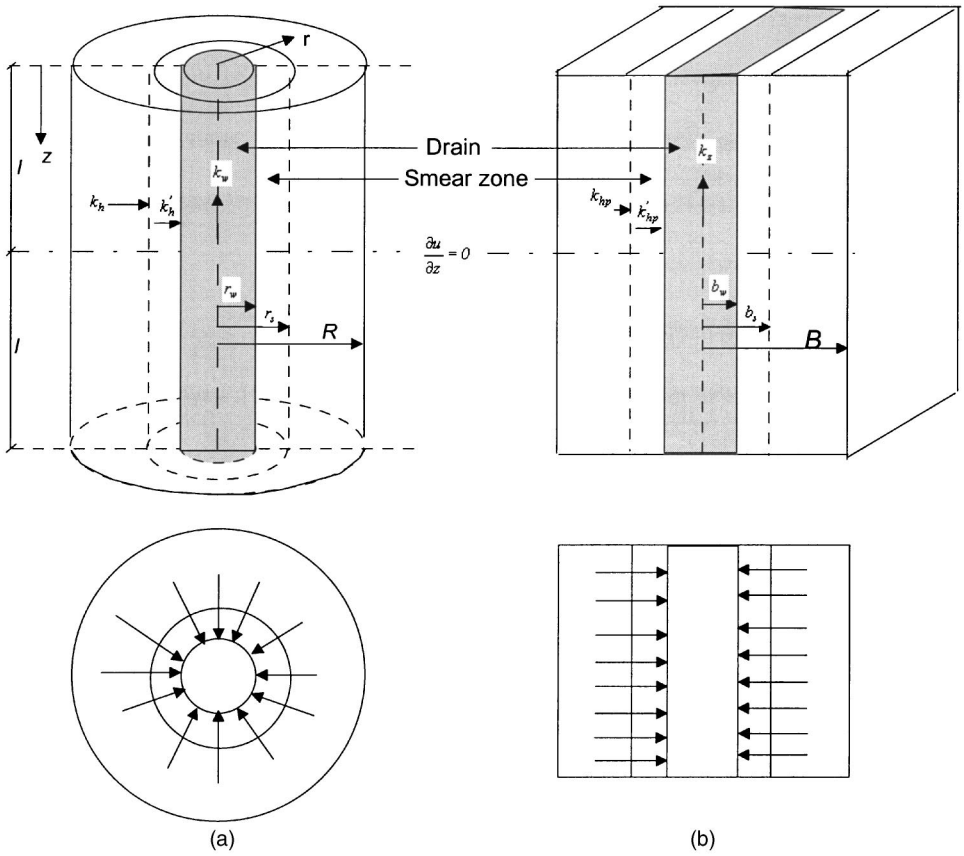

Fig. 1. Conversion of axisymmetric unit cell into plane strain wall: (a) axisymmetric; and (b) plane strain

cation of vacuum pressure with prefabricated vertical drains requires modification of boundary condition of existing theories. In this study, a comprehensive analytical solution for vacuum preloading in conjunction with vertical drains is introduced, under both axisymmetric and equivalent plane strain conditions. The predictions based on the analytical solution are also compared with numerical analysis, which verifies that good agreement exists between both methods.

Analytical Solution for Vertical Drain with Vacuum Preloading

Fig. 1 shows the conversion of an axisymmetric vertical drain into an equivalent drain wall. In this analysis, the coefficient of permeability and applied vacuum pressure are transformed while keeping the geometry of the unit cell the same (i.e., $B=R$, $b_w=r_w$, and $b_s=r_s$). Experience has shown that when vacuum pressure is applied in the field through PVDs, the suction head may decrease with depth as well as laterally, thereby reducing the efficiency. In order to study the effect of vacuum loss, a trapezoidal vacuum pressure distribution is assumed (Fig. 2). In the vertical direction (along the drain boundary), the vacuum pressure varies from $-p_0$ to $-k_1p_0$, while it varies from $-p(z,r_w)$ to $-k_2p(z,r_w)$ across the soil.

Solution for Axisymmetric Condition (Neglecting Well Resistance)

In the following section, the derivations of governing equations are given, where all parameters are defined in the Notation.

The vacuum pressure at any point assuming a linear variation can be written as

$$u_{\text{vac}} = p_0\left[1-(1-k_1)\frac{z}{l}\right]\left[1-(1-k_2)\left(\frac{r-r_w}{R-r_w}\right)\right] \tag{1}$$

Now at any time, the hydraulic head (static pressure head) can be found by

$$h = \frac{1}{\gamma_w}(u+u_{\text{vac}}) = \frac{1}{\gamma_w}\left\{u+p_0\left[1-(1-k_1)\frac{z}{l}\right]\times\left[1-(1-k_2)\left(\frac{r-r_w}{R-r_w}\right)\right]\right\} \tag{2}$$

Differentiating Eq. (2) with respect to radius gives the hydraulic gradient (i)

$$i = \frac{1}{\gamma_w}\left\{\frac{\partial u}{\partial r}-p_0\left[1-(1-k_1)\frac{z}{l}\right](1-k_2)\frac{1}{(R-r_w)}\right\} \tag{3}$$

The flow in the slice at a distance r from the centerline of the drain is equal to the volume change within a block of soil of width $(R-r)$ such that

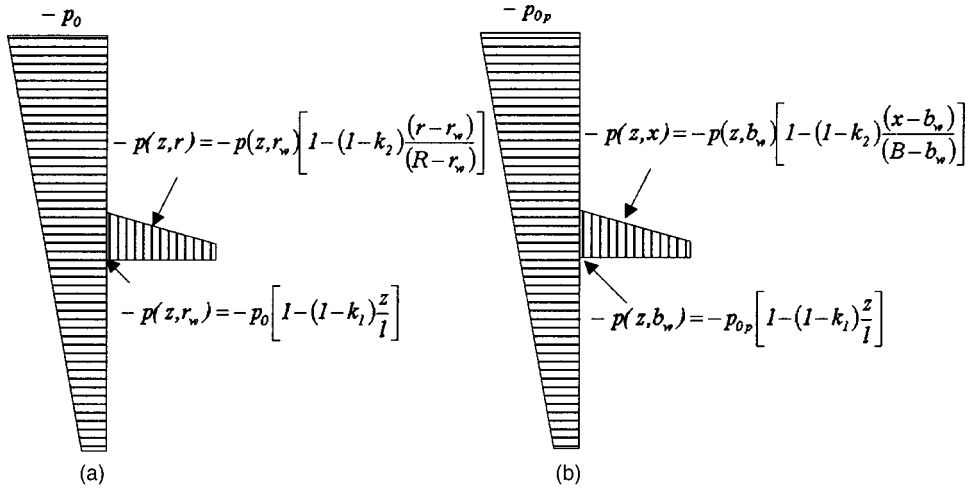

Fig. 2. Vacuum pressure distribution: (a) axisymmetric; and (b) equivalent plane strain based on laboratory observations

$$\frac{\partial Q}{\partial t} = kiA = \frac{k}{\gamma_w}\left\{\frac{\partial u}{\partial r} - p_0\left[1-(1-k_1)\frac{z}{l}\right](1-k_2)\frac{1}{(R-r_w)}\right\}2\pi r\,dz = \frac{\partial \varepsilon}{\partial t}\pi(R^2-r^2)dz \tag{4}$$

By rearranging Eq. (4), the excess pore pressure variation inside and outside the smear zone can be derived as follows:
For $r_w \leqslant r \leqslant r_s$

$$\frac{\partial u'}{\partial r} = \frac{\gamma_w}{2k_h'}\frac{\partial \varepsilon}{\partial t}\left(\frac{R^2-r^2}{r}\right) + p_0\frac{(1-k_2)}{(R-r_w)}\left[1-(1-k_1)\frac{z}{l}\right] \tag{5}$$

For $r_s \leqslant r \leqslant R$

$$\frac{\partial u}{\partial r} = \frac{\gamma_w}{2k_h}\frac{\partial \varepsilon}{\partial t}\left(\frac{R^2-r^2}{r}\right) + p_0\frac{(1-k_2)}{(R-r_w)}\left[1-(1-k_1)\frac{z}{l}\right] \tag{6}$$

Integrating Eq. (5) in the radial direction with the boundary condition $u'_{r=r_w}=p(z,r_w)$, the excess pore pressure within the smear zone is given by

$$u' = \frac{\gamma_w}{2k_h'}\frac{\partial \varepsilon}{\partial t}\left[R^2\ln\left(\frac{r}{r_w}\right) - \frac{(r^2-r_w^2)}{2}\right] - p_0\left[1-(1-k_1)\frac{z}{l}\right] \times\left[1-(1-k_2)\frac{(r-r_w)}{(R-r_w)}\right] \tag{7}$$

Integrating Eq. (6) in the radial direction with the boundary condition $u'_{r=r_s}=u_{r=r_s}$ the excess pore pressure outside the smear zone can be found as

$$u = \frac{\gamma_w}{2k_h}\frac{\partial \varepsilon}{\partial t}\left[R^2\ln\left(\frac{r}{r_s}\right) - \frac{(r^2-r_s^2)}{2}\right] + \frac{\gamma_w}{2k_h'}\frac{\partial \varepsilon}{\partial t}\left[R^2\ln\left(\frac{r_s}{r_w}\right) - \frac{(r_s^2-r_w^2)}{2}\right] - p_0\left[1-(1-k_1)\frac{z}{l}\right]\left[1-(1-k_2)\frac{(r-r_w)}{(R-r_w)}\right] \tag{8}$$

Hence, the average excess pore pressure at a given time is

$$\overline{u} = \frac{\int_0^l\int_{r_w}^{r_s} u'2\pi r\,dr\,dz + \int_0^l\int_{r_s}^{R} u2\pi r\,dr\,dz}{\pi(R^2-r_w^2)l} = \frac{\int_0^l\int_{r_w}^{r_s} u'2r\,dr\,dz + \int_0^l\int_{r_s}^{R} u2r\,dr\,dz}{(R^2-r_w^2)l} \tag{9}$$

By substituting Eqs. (1), (7), and (8) into (9), and rearranging gives

$$\overline{u} = \frac{\partial \varepsilon}{\partial t}\gamma_w\frac{R^2}{2k_h}\mu - p_0G(n) \tag{10a}$$

where

$$G(n) = \frac{(1+k_1)[n(1+2k_2)+(2+k_2)]}{6(n+1)} \tag{10b}$$

$$\mu = \frac{n^2}{n^2-1}\left[\ln\left(\frac{n}{s}\right) + \frac{k_h}{k_h'}\ln(s) - \frac{3}{4}\right] + \frac{s^2}{n^2-1}\left(1-\frac{s^2}{4n^2}\right) + \frac{k_h}{k_h'}\frac{1}{n^2-1}\left(\frac{s^4-1}{4n^2} - s^2 + 1\right) \approx \left[\ln\left(\frac{n}{s}\right) + \frac{k_h}{k_h'}\ln(s) - \frac{3}{4}\right] \tag{10c}$$

Now Eqs. (10*a*)–(10*c*) may be combined with the time-dependent compressibility governed by the following well-known consolidation expression

$$\frac{\partial \varepsilon}{\partial t} = -m_v\frac{\partial \overline{u}}{\partial t} = -\frac{k_h}{c_h\gamma_w}\frac{\partial \overline{u}}{\partial t} \tag{11}$$

By substituting Eqs. (10*a*)–(10*c*) into (11) and rearranging gives

$$-\frac{2c_h}{R^2\mu} = \frac{1}{\overline{u}+p_0G(n)}\frac{\partial \overline{u}}{\partial t} \tag{12}$$

Integrating Eq. (12) subjected to the boundary condition that at $t=0$, $\overline{u}=\overline{u}_0$, leads to

$$\frac{\overline{u}}{\overline{u_0}} = \left(1 + \frac{p_0 G(n)}{\overline{u_0}}\right)\exp\left(-\frac{8T_h}{\mu}\right) - \frac{p_0 G(n)}{\overline{u_0}} \tag{13}$$

the vacuum pressure ratio (VPR) can be introduced by the value of $p_0/\overline{u_0}$ (i.e., applied vacuum pressure/initial excess pore water pressure). It can be noted that to avoid cavitation being negative at 1 atm, VPR may be limited depending on the amount of the initial excess pore water pressure.

By combining Eqs. (7), (11), and (13), the normalized excess pore pressure at any point within the smear zone ($u'/\overline{u_0}$) can be found as

$$\frac{u'}{\overline{u_0}} = \frac{k_h}{k'_h}\frac{1}{\mu R^2}\left(1 + \frac{p_0 G(n)}{\overline{u_0}}\right)\exp\left(-\frac{8T_h}{\mu}\right)\left[R^2 \ln\left(\frac{r}{r_w}\right) - \frac{(r^2 - r_w^2)}{2}\right] - \frac{p_0}{\overline{u_0}}\left[1 - (1 - k_1)\frac{z}{l}\right]\left[1 - (1 - k_2)\frac{(r - r_w)}{(R - r_w)}\right] \tag{14}$$

By combining Eqs. (8), (11), and (13), the normalized excess pore pressure at any point outside the smear zone ($u/\overline{u_0}$) is given by

$$\frac{u}{\overline{u_0}} = \frac{1}{\mu R^2}\left(1 + \frac{p_0 G(n)}{\overline{u_0}}\right)\exp\left(-\frac{8T_h}{\mu}\right)\left\{R^2 \ln\left(\frac{r}{r_s}\right) - \frac{(r^2 - r_s^2)}{2} + \frac{k_h}{k'_h}\left[R^2 \ln\left(\frac{r_s}{r_w}\right) - \frac{(r_s^2 - r_w^2)}{2}\right]\right\} - \frac{p_0}{\overline{u_0}}\left[1 - (1 - k_1)\frac{z}{l}\right]\left[1 - (1 - k_2)\frac{(r - r_w)}{(R - r_w)}\right] \tag{15}$$

Substituting Eq. (14) into Eq. (3), the normalized hydraulic gradient at any point within the smear zone ($i'\gamma_w/\overline{u_0}$) is determined as

$$\frac{i'\gamma_w}{\overline{u_0}} = \frac{k_h}{k'_h}\frac{1}{\mu R}\left(1 + \frac{p_0 G(n)}{\overline{u_0}}\right)\exp\left(-\frac{8T_h}{\mu}\right)\left(\frac{R}{r} - \frac{r}{R}\right) \tag{16}$$

Substituting Eq. (15) into Eq. (3), the normalized hydraulic gradient at any point outside the smear zone ($i\gamma_w/\overline{u_0}$) is derived as

$$\frac{i\gamma_w}{\overline{u_0}} = \frac{1}{\mu R}\left(1 + \frac{p_0 G(n)}{\overline{u_0}}\right)\exp\left(-\frac{8T_h}{\mu}\right)\left(\frac{R}{r} - \frac{r}{R}\right) \tag{17}$$

Equivalent Plane Strain Solution (Neglecting Well Resistance)

The vacuum pressure at any point can be written as (assuming the same gradient)

$$u_{\text{vac},p} = p_{0p}\left[1 - (1 - k_1)\frac{z}{l}\right]\left[1 - (1 - k_2)\left(\frac{x - b_w}{B - b_w}\right)\right] \tag{18}$$

Now at any time, the hydraulic head can be found as

$$h = \frac{1}{\gamma_w}\left\{u + p_{0p}\left[1 - (1 - k_1)\frac{z}{l}\right]\left[1 - (1 - k_2)\left(\frac{x - b_w}{B - b_w}\right)\right]\right\} \tag{19}$$

Differentiating Eq. (19) with respect to distance gives

$$i = \frac{1}{\gamma_w}\left\{\frac{\partial u}{\partial x} - p_{0p}\left[1 - (1 - k_1)\frac{z}{l}\right](1 - k_2)\frac{1}{(B - b_w)}\right\} \tag{20}$$

The flow in the slice at a distance x from the centerline of the drain is equal to the volume change within a block of soil of width $(B-x)$, such that

$$\frac{\partial Q}{\partial t} = kiA = \frac{k}{\gamma_w}\left\{\frac{\partial u}{\partial x} - p_{0p}\left[1 - (1 - k_1)\frac{z}{l}\right](1 - k_2)\frac{1}{(B - b_w)}\right\}dz = \frac{\partial \varepsilon}{\partial t}(B - x)dz \tag{21}$$

By rearranging Eq. (21), the excess pore pressure variations inside and outside the smear zone are determined by

$$\frac{\partial u'}{\partial x} = \frac{\gamma_w}{k'_{\text{hp}}}\frac{\partial \varepsilon}{\partial t}(B - x) + p_{0p}\frac{(1 - k_2)}{(B - b_w)}\left[1 - (1 - k_1)\frac{z}{l}\right] \tag{22}$$

$$\frac{\partial u}{\partial x} = \frac{\gamma_w}{k_{\text{hp}}}\frac{\partial \varepsilon}{\partial t}(B - x) + p_{0p}\frac{(1 - k_2)}{(B - b_w)}\left[1 - (1 - k_1)\frac{z}{l}\right] \tag{23}$$

Integrating Eq. (22) in the x direction with the boundary condition $u'_{x=b_w} = p(z, b_w)$, the excess pore pressure within the smear zone is derived as

$$u' = \frac{\gamma_w}{2k'_{\text{hp}}}\frac{\partial \varepsilon}{\partial t}[x(2B - x) - b_w(2B - b_w)] - p_{0p}\left[1 - (1 - k_1)\frac{z}{l}\right]\left[1 - (1 - k_2)\frac{(x - b_w)}{(B - b_w)}\right] \tag{24}$$

Integrating Eq. (23) in the x direction with the boundary condition $u'_{x=b_s} = u_{x=b_s}$, the excess pore pressure outside the smear zone can be found as

$$u = \frac{\gamma_w}{2k_{\text{hp}}}\frac{\partial \varepsilon}{\partial t}\left[x(2B - x) - b_s(2B - b_s) + \frac{k_{\text{hp}}}{k'_{\text{hp}}}(b_s - b_w)(2B - b_s - b_w)\right] - p_{0p}\left[1 - (1 - k_1)\frac{z}{l}\right]\left[1 - (1 - k_2)\frac{(x - b_w)}{(B - b_w)}\right] \tag{25}$$

Hence, the average excess pore pressure at a given time is

$$\overline{u} = \frac{\int_0^l \int_{b_w}^{b_s} u'\,dx\,dz + \int_0^l \int_{b_s}^{B} u\,dx\,dz}{(B - b_w)l} \tag{26}$$

By substituting Eqs. (18), (24), and (25) into Eq. (26), and rearranging gives

$$\overline{u} = \frac{\partial \varepsilon}{\partial t}\gamma_w \frac{B^2}{2k_{\text{hp}}}\mu_p - p_{0p}\frac{(1 + k_1)(1 + k_2)}{4} \tag{27a}$$

In the above equation

$$\mu_p = \left[\alpha + \frac{k_{\text{hp}}}{k'_{\text{hp}}}\beta\right]$$

$$\alpha = \frac{2}{3}\frac{(n - s)^3}{n^2(n - 1)}$$

and

$$\beta = \frac{2(s - 1)}{n^2(n - 1)}\left[n(n - s - 1) + \frac{1}{3}(s^2 + s + 1)\right] \tag{27b}$$

Eqs. (27*a*) and (27*b*) may now be combined with the time-dependent compressibility governed by the following well-known consolidation expression

$$\frac{\partial \varepsilon}{\partial t} = -m_v \frac{\partial \overline{u}}{\partial t} = -\frac{k_{\text{hp}}}{c_h \gamma_w}\frac{\partial \overline{u}}{\partial t} \tag{28}$$

By substituting Eq. (27) into (28) and rearranging yields

$$-\frac{2c_{hp}}{B^2\mu_p}=\frac{1}{\overline{u}+p_{0p}\dfrac{(1+k_1)(1+k_2)}{4}}\frac{\partial\overline{u}}{\partial t} \tag{29}$$

Integrating Eq. (29) subjected to the boundary condition that at $t=0$, $\overline{u}=\overline{u_0}$ leads to

$$\frac{\overline{u}}{\overline{u_0}}=\left(1+\frac{p_{0p}}{\overline{u_0}}\frac{(1+k_1)(1+k_2)}{4}\right)\exp\left(-\frac{8T_{hp}}{\mu_p}\right)-\frac{p_{0p}}{\overline{u_0}}\frac{(1+k_1)(1+k_2)}{4} \tag{30}$$

By combining Eqs. (24), (28), and (30), the normalized excess pore pressure at any point inside the smear zone $(u'/\overline{u_0})$ can be found as

$$\begin{aligned}\frac{u'}{\overline{u_0}}=&\frac{k_{hp}}{k'_{hp}}\frac{1}{\mu_p B^2}\left[1+\frac{p_{0p}}{\overline{u_0}}\frac{(1+k_1)(1+k_2)}{4}\right]\\&\times\exp\left(-\frac{8T_{hp}}{\mu_p}\right)[x(2B-x)-b_w(2B-b_w)]\\&-\frac{p_{0p}}{\overline{u_0}}\left[1-(1-k_1)\frac{z}{l}\right]\left[1-(1-k_2)\frac{(x-b_w)}{(B-b_w)}\right]\end{aligned} \tag{31}$$

By combining Eqs. (25), (28), and (30), the normalized excess pore pressure at any point outside the smear zone $(u/\overline{u_0})$ can be determined by

$$\begin{aligned}\frac{u}{\overline{u_0}}=&\frac{1}{B^2\mu_p}\left[1+\frac{p_{0p}}{\overline{u_0}}\frac{(1+k_1)(1+k_2)}{4}\right]\\&\times\exp\left(-\frac{8T_{hp}}{\mu_p}\right)\left[\begin{array}{c}x(2B-x)-b_s(2B-b_s)\\+\\\dfrac{k_{hp}}{k'_{hp}}(b_s-b_w)(2B-b_s-b_w)\end{array}\right]\\&-\frac{p_{0p}}{\overline{u_0}}\left[1-(1-k_1)\frac{z}{l}\right]\left[1-(1-k_2)\frac{(x-b_w)}{(B-b_w)}\right]\end{aligned} \tag{32}$$

Substituting Eq. (31) into Eq. (20), the normalized hydraulic gradient at any point within $(i'\gamma_w/\overline{u_0})$ the smear zone is represented by

$$\begin{aligned}\frac{i'\gamma_w}{\overline{u_0}}=&\frac{2k_{hp}}{k'_{hp}}\frac{1}{\mu_p B}\left[1+\frac{p_{0p}}{\overline{u_0}}\frac{(1+k_1)(1+k_2)}{4}\right]\\&\times\exp\left(-\frac{8T_{hp}}{\mu_p}\right)\left(1-\frac{x}{B}\right)\end{aligned} \tag{33}$$

Substituting Eq. (32) into Eq. (20), the normalized hydraulic gradient at any point outside the smear zone $(i\gamma_w/\overline{u_0})$ is given by

$$\frac{i\gamma_w}{\overline{u_0}}=\frac{2}{\mu_p B}\left[1+\frac{p_{0p}}{\overline{u_0}}\frac{(1+k_1)(1+k_2)}{4}\right]\exp\left(-\frac{8T_{hp}}{\mu_p}\right)\left(1-\frac{x}{B}\right) \tag{34}$$

Equivalent Plane Strain Parameters

To obtain the same degree of consolidation at a certain time under both axisymmetric and plane strain conditions, the constant term and the exponential term in Eqs. (13) and (30) should be equal. Therefore,

$$\frac{p_{0p}}{\overline{u_0}}\frac{(1+k_1)(1+k_2)}{4}=\frac{p_0G(n)}{\overline{u_0}} \tag{35a}$$

and

$$\frac{T_{hp}}{\mu_p}=\frac{T_h}{\mu} \tag{35b}$$

From Eq. (35*a*), the equivalent vacuum pressure under plane strain is

$$p_{0p}=p_0\frac{2[n(1+2k_2)+(2+k_2)]}{3(n+1)(1+k_2)} \tag{36}$$

From Eq. (35*b*), the equivalent permeability under plane strain is given by

$$\frac{k_{hp}}{k_h}=\frac{\left[\alpha+\dfrac{k_{hp}}{k'_{hp}}\beta\right]}{\left[\ln\left(\dfrac{n}{s}\right)+\dfrac{k_h}{k'_h}\ln(s)-\dfrac{3}{4}\right]} \tag{37}$$

where α and β have been defined earlier [see Eq. (27*b*)]

Now, by neglecting the smear effect, the equivalent permeability outside the smear zone can be derived as

$$\frac{k_{hp}}{k_h}=\frac{[\alpha+\beta]}{[\ln(n)-0.75]}=\frac{\left[\dfrac{2}{3}\left(1-\dfrac{1}{n}\right)^2\right]}{[\ln(n)-0.75]}\approx\frac{0.67}{[\ln(n)-0.75]} \tag{38}$$

By rearranging Eq. (37), the equivalent permeability within the smear zone can be determined by

$$\frac{k'_{hp}}{k_{hp}}=\frac{\beta}{\dfrac{k_{hp}}{k_h}\left[\ln\left(\dfrac{n}{s}\right)+\dfrac{k_h}{k'_h}\ln(s)-\dfrac{3}{4}\right]-\alpha} \tag{39}$$

Note that by substituting p_0 (or u_{vac})$=0$ in Eqs. (13)–(17), Hansbo's (1981) original solution can be obtained, whereas by substituting p_{0_p} (or $u_{vac,p}$)$=0$ in Eqs. (30) and (34), the solution proposed by Indraratna and Redana (2000) can be derived.

Comparison Between Results of Two Theories

Without Vacuum Preloading

In order to verify that the proposed plane strain solution compares well with the axisymmetric solution, a unit cell analysis is performed with the following parameters: $R=B=0.5$ m, $r_w=b_w=0.03$ m, $r_s=b_s=0.09$ m, $k_h=0.03$ m/year, $k'_h=0.01$ m/year, and $c_h=1$ m^2/year. The plane strain parameters are calculated from Eqs. (38) and (39) as follows: $k_{hp}=8.52\times10^{-3}$ m/s and $k'_{hp}=2.09\times10^{-3}$ m/s. Fig. 3 shows the normalized excess pore pressure variation with time at a distance $2r_s$ (outside the smear zone) and $0.5r_s$ (inside the smear zone). This result shows that the analysis based on the plane strain solution is very close to the axisymmetric solution. The normalized excess pore pressure variation with the radial (horizontal) distance is plotted in Fig. 4 after 90 days. This result reaffirms that the equivalent plane strain solution can be applied in confidence to the actual axisymmetric problem.

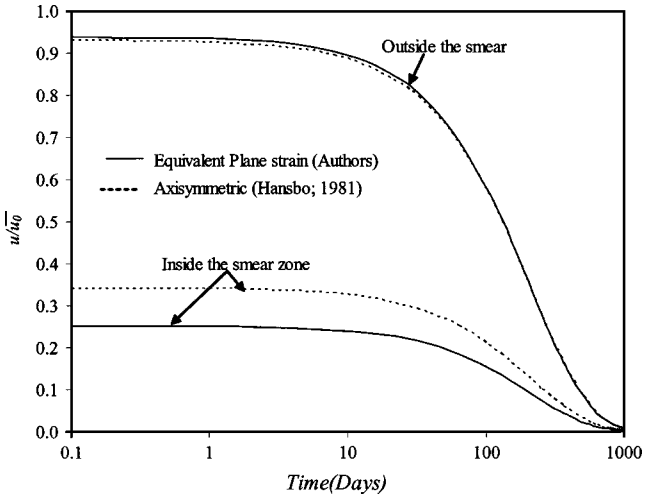

Fig. 3. Normalized excess pore pressure variation with time at points $2r_s$ and $0.5r_s$

With Vacuum Preloading

Experience has shown that when vacuum pressure is applied in the field through PVDs, the suction head along the drain length may decrease with depth, thereby reducing the efficiency (Chu et al. 2000). In the case of short vertical drains, the laboratory measurements at a few points along the drain in the large-scale consolidometer clearly indicated that the vacuum pressure definitely decreases down the drain length (Indraratna et al. 2004). Therefore, the results attributed to axisymmetric and equivalent plane strain conditions, are compared by assuming four distinctly different vacuum pressure distributions:

1. Case A: vacuum pressure is constant throughout the layer ($k_1=k_2=1$);
2. Case B: vaccum pressure is kept constant along the drain, while it varies linearly to zero across the soil ($k_1=1, k_2=0$);
3. Case C: vacuum pressure is maintained constant across the soil, while it varies linearly to zero along the drain length ($k_1=0, k_2=1$); and
4. Case D: vacuum pressure varies linearly along the drain length as well as across the soil element ($k_1=k_2=0$).

The following parameters are used for this analysis: $n=20$, $s=6$, and $k_h/k_h'=10$. Fig. 5 shows a comparison of normalized excess pore-water pressure with time factor for the four different combinations of vacuum pressure distributions (VPR is taken as 1). As expected, the dissipation of excess pore-water pressure with the applied vacuum pressure is faster than the case without any vacuum pressure. Based on laboratory observations (e.g., Indraratna et al. 2004), the assumption of varying vacuum pressure along the drain length (Case C) is more realistic, as the effect of vacuum pressure usually diminishes with depth (Fig. 2).

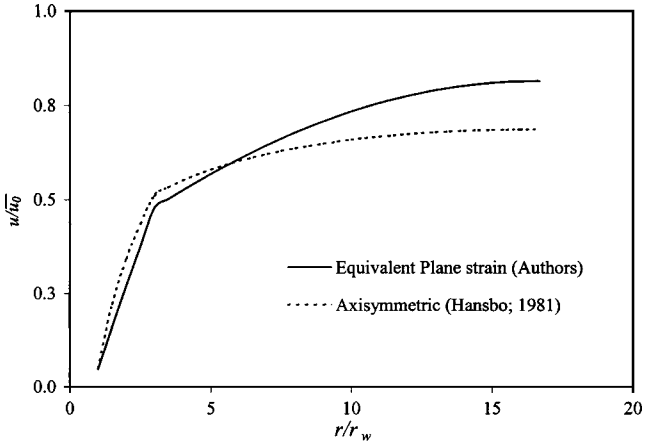

Fig. 4. Normalized excess pore pressure variation with radial (horizontal) direction after 90 days

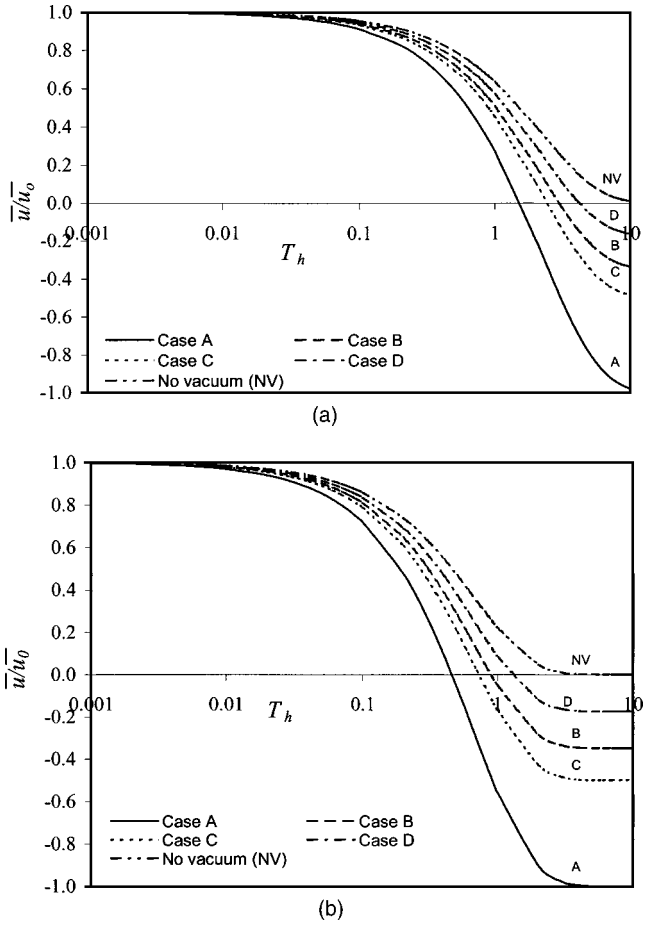

Fig. 5. Comparison of normalized excess pore pressure for various vacuum pressure distribution for vacuum pressure ratio=1: (a) axisymmetric solution; and (b) plane strain solution

The effect of the magnitude of applied vacuum pressure is illustrated in Fig. 6 for Case C. It is clear that greater the magnitude of vacuum pressure, the higher the rate of consolidation. Unless the magnitude of vacuum pressure is large enough, the effect on pore pressure dissipation may not be significant. From Fig. 6, it can be noted that the efficiency of vertical drains with vacuum preloading depends on both the distribution and magnitude of the applied vacuum pressure.

Application of Model to Case History

The Second Bangkok International Airport is located about 30 km east of Bangkok, Thailand and the subsoil layer at this site is composed of a thick soft clay deposit. Due to the high annual rainfall on this low-lying ground, the soil generally retains a very high moisture content. Several test embankments were con-

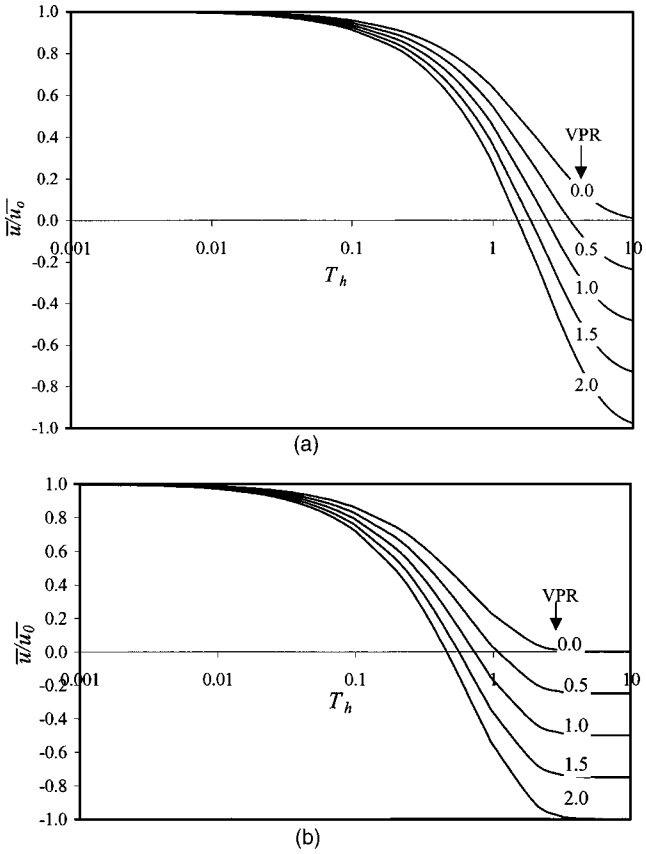

Fig. 6. Effect of varying vacuum pressure ratios on normalized excess pore pressure (for Case C): (a) axisymmetric solution; and (b) plane strain solution

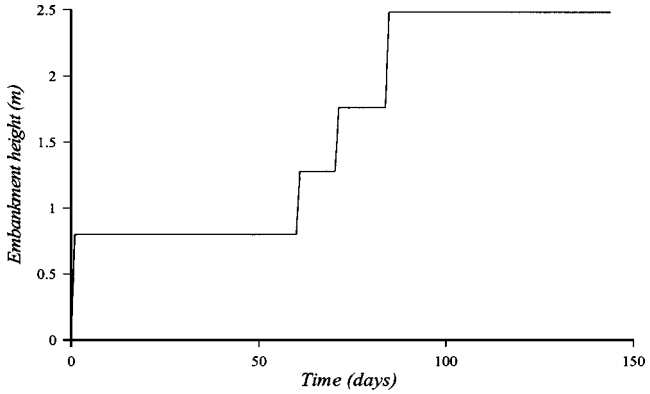

Fig. 8. Construction loading history of embankment

structed on soft Bangkok clay, a few with vacuum preloading and PVD systems. In this paper, the behavior of a selected embankment TV2 is analyzed in detail. The field measurements (Asian Institute of Technology 1995) are compared with the numerical prediction. The total base area of the embankment was 40 $\times$ 40 m^2 and its vertical cross section is shown in Fig. 7. For embankment TV2, 12 m long PVDs with perforated and corrugated pipes combined with nonwoven geotextile were utilized. The drainage blanket which serves as a working platform was constructed with sand to a thickness of 0.8 m. A water and air tight linear low density polyethylene geomembrane liner was placed on top of the drainage system. The borders of the geomembrane liner was completely sealed off from the atmosphere by placing the liner borders at the bottom of the trench. At the bottom of the trench, a 0.30 m thick layer of sand–bentonite was placed. The water collection system in each embankment was connected to a vacuum pump having a capability of supplying continuous vacuum pressure. The PVDs were installed in a triangular pattern with 1.0 m spacing and the equivalent drain diameter was 50 mm. In this study, the extent of smear zone was taken as six times the equivalent drain diameter, and the discharge ca-

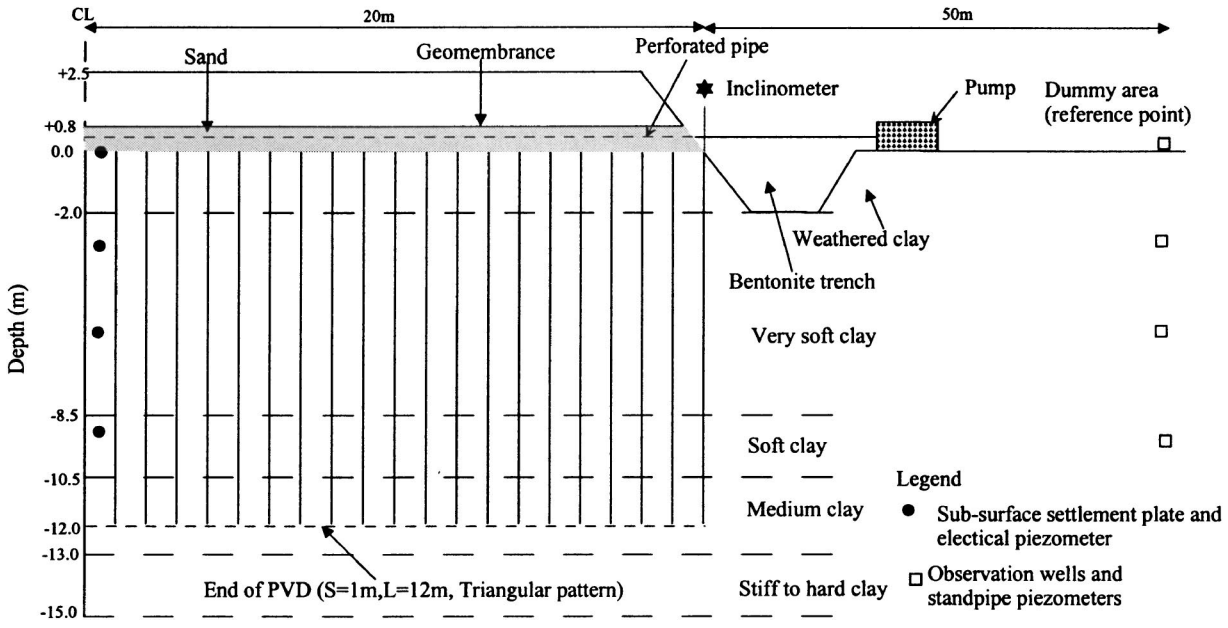

Fig. 7. Cross section of test embankment with subsoil profile, Second Bangkok International Airport, Thailand

Table 1. Selected Soil Parameters in Finite Element Method Analysis

Depth (m)	λ	κ	ν	e_0	γ (kN/m^3)	k_v (10^{-9} m/s)	k_h (10^{-9} m/s)	k'_h (10^{-9} m/s)	k_{hp} (10^{-9} m/s)	k'_{hp} (10^{-9} m/s)
0.0–2.0	0.3	0.03	0.30	1.8	16	15.1	30.1	15.1	9.0	3.45
2.0–8.5	0.7	0.08	0.30	2.8	15	6.4	12.7	6.4	3.8	1.46
8.5–10.5	0.5	0.05	0.25	2.4	15	3.0	6.0	3.0	1.8	0.69
10.5–13.0	0.3	0.03	0.25	1.8	16	1.3	2.6	1.3	0.8	0.30
13.0–15.0	1.2	0.10	0.25	1.2	18	0.3	0.6	0.3	0.2	0.07

pacity of the drain was estimated to be about 50 m^3/year based on a single drain analysis conducted recently by Indraratna and Sathananthan (2003).

A vacuum pump capable of generating 70 kPa suction pressure was employed, and after 45 days of vacuum application, the embankment was raised in four stages up to a height of 2.5 m (the unit weight of surcharge fill was 18 kN/m^3). The loading stage of the embankment is illustrated in Fig. 8. A comprehensive instrumentation scheme including surface settlement plates, subsurface multipoint extensometers, vibrating wire electrical piezometers, and inclinometers were installed to monitor the embankment behavior (Fig. 7). The surface settlement plates were placed directly on top of the geomembrane at the centerline of the embankment, and an inclinometer was installed at the edges of the embankment. The vibrating wire piezometers were installed under the test embankment at 3 m depth intervals, and at 0.5 m away from the centerline, together with the sensors for the multipoint piezometer. At the dummy area, the place where it is not disturbed by the embankment construction, observation wells and standpipe piezometers were installed to obtain the reference data to compare with field results (Fig. 7). The settlement, excess pore water pressure and lateral movement were monitored for about 150 days.

The numerical analysis was based on the modified Cam-clay model and the equivalent plane strain Eqs. (36)–(39) were incorporated in the finite element code, *ABAQUS*. The adopted parameters of subsoil layers based on the laboratory testings are listed in Table 1. According to Indraratna and Redana (1998), the extent of the smear zone can be determined by measuring the change of k_h/k_v ratio of soil surrounding the vertical drain. In the analysis, the extent of smear zones was 300 mm based on the previous case histories constructed at the same site (Indraratna and Redana 2000). For the plane strain simulation, the equivalent permeability inside and outside the smear zone was calculated using Eqs. (38) and (39). The finite element mesh, which contained eight-node biquadratic displacement and bilinear pore pressure elements, is shown in Fig. 9. Because of symmetry, it was sufficient to consider one half of the embankment for the finite element analysis. For the area with PVDs and smear zone, a finer mesh was employed so that each unit cell represented a single drain and the smear zone on either side of the drain. The finer mesh also prevented any unfavorable aspect ratio of the elements. The embankment loading was simulated by applying incremental vertical loads to the upper boundary.

The field measurements reported by AIT (1995) were compared with the numerical predictions. Fig. 10 illustrates the measured pore pressure at various depths for the embankment from electrical piezometers installed 0.5 m away from the centerline. After 40 days, a discrepancy between the measured and applied vacuum pressure is noted. The suction head in the field could not be maintained because of possible air leaks. Therefore, in the numerical analysis, the magnitude of applied vacuum pressure at the surface was adjusted based on the field measurements. Fig. 11 shows the assumed variation of vacuum pressure applied at the surface with time. The lateral and vertical distributions of applied

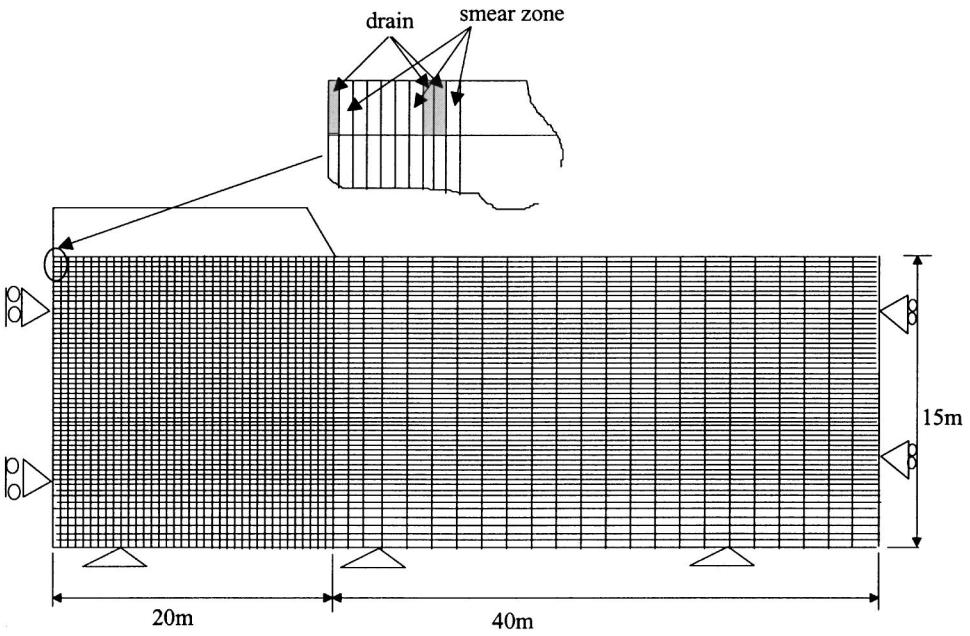

Fig. 9. Finite element mesh for plane strain analysis

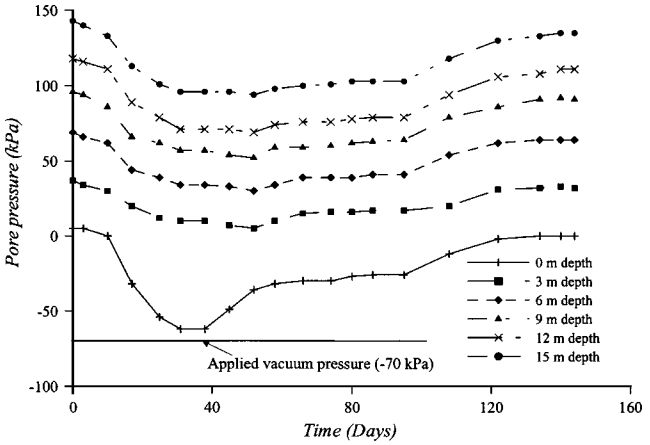

Fig. 10. Measured pore pressure variation with time and depth, 0.5 m away from centerline

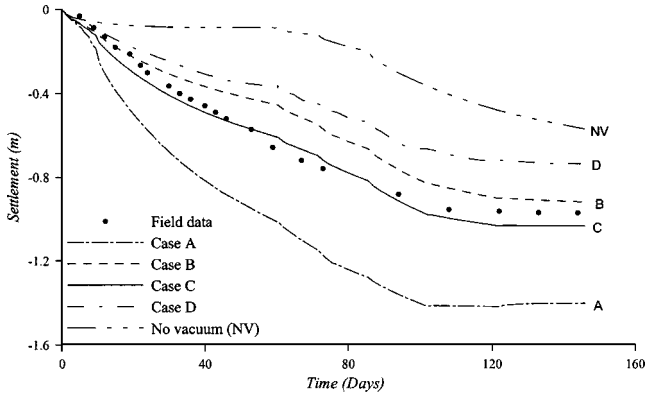

Fig. 12. Surface settlement of embankment (at centerline)

vacuum pressure were considered among four possible cases (A–D) as explained earlier.

Based on plane strain multidrain analysis, Fig. 12 illustrates the comparison between the predicted surface settlement (centerline) and the measured data for Cases A–D. Case C predictions seem to agree best with the measured results. Fig. 13 shows the comparison between Case C predictions and the field measurements at various depths at the centerline. Comparing all categories of vacuum pressure distributions, Case A and "no vacuum pressure" give the highest and lowest settlement, respectively. It is shown that the vacuum application in conjunction with a PVD system can significantly accelerate the consolidation process, and most of the primary consolidation with vacuum application is achieved around 120 days, whereas the conventional case requires further time to reach the end of primary consolidation (after 150 days).

It is expected that for relatively long PVDs, the effect of vacuum pressure application may diminish along the length of the drain [based on laboratory observations (Indraratna et al. 2004)]. From the field measurements and finite element method analysis, it is clear that the pattern of vacuum distribution directly influences the soil consolidation behavior, hence the accuracy of the numerical predictions is governed by the correct assumption of vacuum pressure distribution in both vertical and lateral directions.

The comparisons between predicted and measured excess pore pressure and lateral movement (at the end of construction) are shown in Figs. 14 and 15, respectively. Fig. 14 illustrates the excess pore-water pressure variation with time for Cases A–D. The field data plot closest to Case C, indicating that the assumption of constant vacuum pressure distribution over the soil surface and linearly decreasing vacuum pressure along the drain length is justified. Unlike settlement, the observed lateral displacements are not matched very well by the vacuum pressure distribution models, but at the middle of the very soft clay layer (4–5 m depth), Case C predictions are still the closest to the field data. In particular, nearer to the ground surface, the field observations do not support the significant "inward" lateral movements as indicated by the numerical predictions. The discrepancy between the predicted and measured results is pronounced in the weathered crust layer (about 0–2 m depth). Previous studies on embankments constucted on soft clay have shown that the accurate prediction of lateral movement is a difficult task, in comparison with vertical displacement (Tavenas et al. 1979). The errors made in the prediction of lateral movements can be numerous, attributed to soil anisotropy and the assumption of 2D plane strain. The embankment corner effects are not properly modeled in 2D plane strain. The behavior of the stiff crust just below the ground surface cannot be modeled using the conventional Cam-clay properties, but

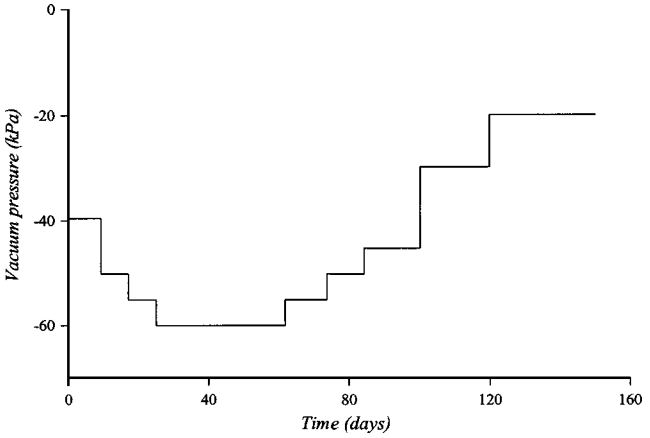

Fig. 11. Assumed vacuum pressure variation at surface applied in finite element analysis

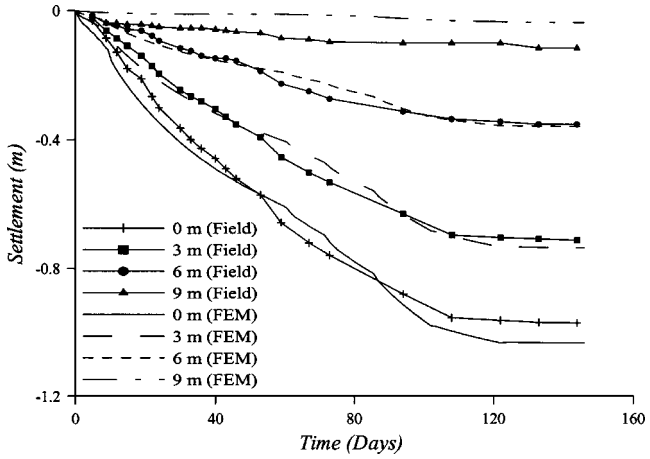

Fig. 13. Settlement of embankment at various depths at centerline (Case C)

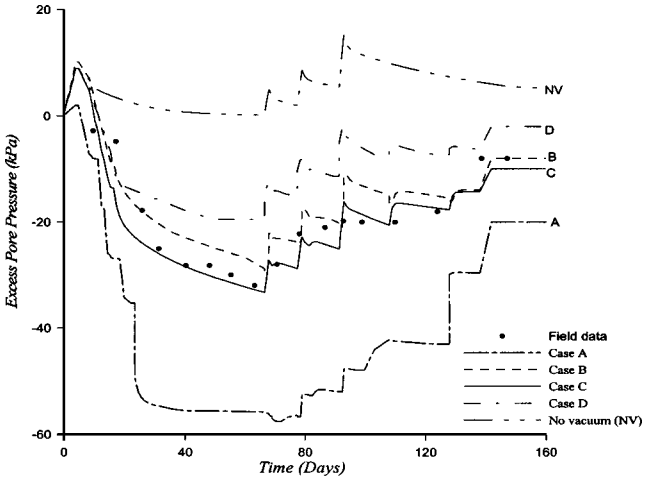

Fig. 14. Excess pore pressure variation at 3 m depth below ground level, 0.5 m away from centerline

requires the accurate assessment of its highly overconsolidated (compacted) properties as discussed in the past by Indraratna et al. (1994). In addition, the comparison between Cases A–D with and without vacuum application confirms that vacuum preloading causes a substantial inward lateral movement of soft soil towards the embankment centerline (i.e., negative displacement in Fig. 15).

Conclusions

In this paper, a modified consolidation theory for vertical drains incorporating vacuum preloading and smear effect has been developed for both axisymmetric and plane strain conditions. Simulating the consolidation of a unit cell surrounding a single vertical drain, a matching procedure based on the transformation of permeability and applied vacuum pressure was introduced to establish the relationships between the axisymmetric and the equivalent plane stain conditions. Four distinct combinations of vacuum pressure distributions (across the soil and along the drain length) were considered in the numerical modeling (i.e., Cases A–D). The results indicate that the efficiency of vertical drains depends on both the magnitude of vacuum pressure and its distribution.

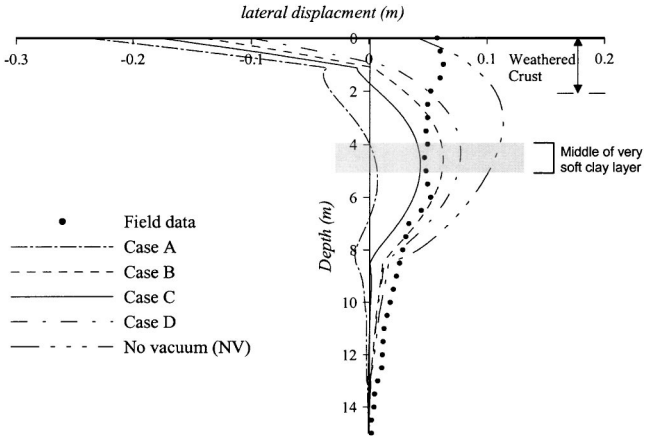

Fig. 15. Predicted and measured lateral displacements at edge of embankment

The finite element (multidrain) analysis based on the plane strain theory was executed to evaluate the performance of a selected full scale embankment on soft Bangkok clay, using the finite element code *ABAQUS*. The effects of both smear and well resistance associated with the PVD were also considered, in conjunction with the applied surcharge load and vacuum pressure. By employing the equivalent plane strain matching procedure, the centerline settlement at different depths, excess pore-water pressure, and lateral movement of the soil were analyzed and compared to the available field data. Case C predictions agreed well with the field observations, except for the lateral displacements at the surface crust. This implies that the assumption of a constant vacuum pressure distribution across the soil and linearly decreasing vacuum pressure along the drain length is realistic, if the drain spacing is sufficiently close (i.e., at 1.0 m).

The accurate prediction of lateral displacement requires careful examination of soil properties for the topmost overconsolidated crust. This compacted layer (up to 2 m) resists the "inward" movement of the soil upon the application of vacuum pressure. The modified Cam-clay model is not appropriate to model the behavior of a thin weathered and compacted crust due to the limitations including soil fabric and anisotropy. In general, vacuum application substantially decreases the lateral displacement, thereby minimizing the risk of shear failure for a given surcharge load.

It can be concluded that the system of PVD subjected to vacuum preloading is a useful method for accelerating radial consolidation and for reducing the surcharge load, as long as the possible air leaks in the field can be prevented. While the finite element simulation discussed here is a useful tool to predict the performance of soft clay stabilized by PVDs, the accurate modelling of vacuum pressure preloading requires further field studies to examine the correct distribution of vacuum pressure within a given soil formation and PVD system, apart from the need for assessing and preventing potential air leaks in practice that may reduce the desirable negative pressure (suction) with time.

Notation

The following symbols are used in the paper:

A = cross sectional area (m^2);
a = width of band drain (m);
B = equivalent half width of plane strain cell (m);
b = thickness of band drain (m);
b_s = equivalent half width of smear zone in plane strain (m);
b_w = equivalent half width of drain (well) in plane strain (m);
c_h = coefficient of horizontal consolidation (m^2/s);
D = diameter of effective influence zone of drain (m);
d_e = equivalent diameter of band drain (m);
d_s = diameter of smear zone (m);
d_w = diameter of drain (well) (m);
$G(n)$ = efficiency of vacuum preloading;
h = hydraulic head (m);
i = hydraulic gradient;
i' = hydraulic gradient in smear zone;
k = permeability (m/s);
k_h = horizontal coefficient of permeability for axisymmetry in undisturbed zone (m/s);

k'_h = horizontal coefficient of permeability for axisymmetry in smear zone (m/s);
k_{hp} = equivalent horizontal coefficient of permeability for plane strain in undisturbed zone (m/s);
k'_{hp} = equivalent horizontal coefficient of permeability for plane strain in smear zone (m/s);
k_v = vertical coefficient of permeability (m/s);
k_1 = vacuum reduction factor in vertical direction;
k_2 = vacuum reduction factor in horizontal direction;
l = length of drain (m);
m_v = coefficient of volume change (m^2/kN);
n = spacing ratio, R/r_w or B/b_w;
p_0 = applied vacuum pressure at top of drain (kN/m^2);
p_{0p} = equivalent vacuum pressure used in plane strain analysis (kN/m^2);
Q = volume of flow (m^3);
R = radius of axisymmetric unit cell (m);
r = radius (m);
r_s = radius of smear zone (m);
r_w = radius of vertical drain (well) (m);
s = smear ratio, r_s/r_w or b_s/b_w;
T_h = time factor for horizontal drainage in axisymmetry;
T_{hp} = time factor for horizontal drainage in plane strain;
t = time (s);
u = excess pore-water pressure outside smear zone (kPa);
u' = excess pore-water pressure inside smear zone (kPa);
$\overline{u}$ = average excess pore pressure (kPa);
$\overline{u_0}$ = initial excess pore-water pressure (kPa);
u_{vac} = applied vacuum pressure in axisymmetric condition (kPa);
$u_{vac,p}$ = applied vacuum pressure in plane strain condition (kPa);
x = distance from centerline for unit cell (plane strain) (m);
z = depth (thickness) of soil layer (m);
α = geometric parameter representing smear in plane strain;
β = geometric parameter representing smear in plane strain;
γ_w = unit weight of water (kN/m^3);
ε = vertical strain;
μ = smear and well resistance factor in axisymmetric; and
μ_p = smear and well resistance factor in plane strain.

References

Asian Institute of Technology (AIT). (1995). "The full-scale field test of prefabricated vertical drains for the Second Bangkok International Airport." *Final Rep.*, Vol. 1, Bangkok, Thailand.

Barron, R. A. (1948). "Consolidation of fine-grained soils by drain wells." *Trans. Am. Soc. Civ. Eng.*, 113, 718–724.

Chu, J., Yan, S. W., and Yang, H. (2000). "Soil improvement by the vacuum preloading method for an oil storage station." *Geotechnique*, 50(6), 625–632.

Cognon, J. M., Juran, I., and Thevanayagam, S. (1994). "Vacuum consolidation technology—Principles and field experience." *Proc., Conf. on Vertical and Horizontal Deformations of Foundations and Embankments Deformations*, College Station, Tex., 1237–1248.

Eriksson, U., Hansbo, S., and Torstensson, B. A. (2000). "Soil improvement at Stockholm–Arlanda Airport." *Ground Improvement*, ICE, U.K., 4, 73–80.

Hansbo, S. (1981). "Consolidation of fine-grained soils by prefabricated drains." *Proc., 10th Int. Conf. SMFE.*, Vol. 3, Stockholm, Sweden, 677–682.

Hird, C. C., Pyrah, I. C., and Russell, D. (1992). "Finite element modelling of vertical drains beneath embankments on soft ground." *Geotechnique*, 42(3), 499–511.

Holtz, R. D., and Christopher, B. R. (1987). "Characteristics of prefabricated drains for accelerating consolidation." *Proc., 9th European Conf. on Soil Mechanics and Foundation Engineering*, Vol. 2, Dublin, Ireland, 903–906.

Indraratna, B., Balasubramaniam, A. S., and Ratnayake, P. (1994). "Performance of embankment stabilized with vertical drains on soft clay." *J. Geotech. Eng.*, 120(2), 257–273.

Indraratna, B., Bamunawita, C., and Khabbaz, H. (2004). "Numerical modeling of vacuum preloading and field applications." *Can. Geotech. J.*, 41(6), 1098–1110.

Indraratna, B., and Redana, I. W. (1997). "Plane strain modeling of smear effects associated with vertical drains." *J. Geotech. Geoenviron. Eng.* 123(5), 474–478.

Indraratna, B., and Redana, I. W. (1998). "Laboratory determination of smear zone due to vertical drain installation." *J. Geotech. Geoenviron. Eng.* 124(2), 180–184.

Indraratna, B., and Redana, I. W. (2000). "Numerical modelling of vertical drains with smear and well resistance installed in soft clay." *Can. Geotech. J.*, 37, 132–145.

Indraratna, B., and Sathananthan, I. (2003). "Comparison of field measurements and predicted performance beneath full-scale embankments." *Proc., 6th Int. Symp. on Field Measurements in GeoMechanics*, Oslo, Norway, 117–127.

Jamiolkowski, M., and Lancellotta, R. (1984). "Embankment on vertical drains: Pore pressure during construction." *Proc., Int. Conf. Case Histories in Geotechnical Engineering*, St. Louis, 275–278.

Kjellman, W. (1952). "Consolidation of clayey soils by atmospheric pressure." *Proc., Conf. on Soil Stabilization*, Massachusetts Institute of Technology, Boston, 258–263.

Mohamedelhassan, E., and Shang, J. Q. (2002). "Vacuum and surcharge combined one-dimensional consolidation of clay soils." *Can. Geotech. J.*, 39, 1126–1138.

Onoue, A. (1988). "Consolidation by vertical drains taking well resistance and smear into consideration." *Soils Found.*, 28(4), 165–174.

Qian, J. H., Zhao, W. B., Cheung, Y. K., and Lee, P. K. K. (1992). "The theory and practice of vacuum preloading." *Comput. Geotech.* 13, 103–118.

Tavenas, F., Mieussens, C., and Bourges, F. (1979). "Lateral displacements in clay foundations under embankments." *Can. Geotech. J.*, 16, 532–550.

Yoshikuni, H., and Nakanodo, H. (1974). "Consolidation of fine-grained soils by drain wells with finite permeability." *Jpn. Soc. Soil Mech. Found. Eng.*, 14(2), 35–46.

Zeng, G. X., and Xie, K. H. (1989). "New development of the vertical drain theories." *Proc., 12th Int. Conf. on Soil Mechanics and Foundation Engineering*, Vol. 2, Rotterdam, The Netherlands, 1435–1438.